Single Null Divertor in Negative Triangularity Tokamak

S.Yu. Medvedev[1,2], M. Kikuchi[3,4,8], T. Takizuka[5], A.A. Ivanov[1], A.A. Martynov[1], Yu.Yu. Poshekhonov[1], A. Merle[6], O. Sauter[6], L. Villard[6], D. Chen[7], J. Jiang[7], J.X. Li[8], J. Zheng[8], T. Ando[9]

[1]Keldysh Institute of Applied Mathematics, RAS, Russia
[2]National Research Nuclear University MEPhI, Russia
[3] National Institutes for Quantum and Radiological Science and Technology, Japan
[4]Institute of Laser Engineering, Osaka University, Japan
[5]Graduate School of Engineering, Osaka University, Japan
[6]Swiss Plasma Center, EPFL, Switzerland
[7]Institute of Nuclear Energy Safety Technology, CAS, China
[8]South Western Institute of Physics, China
[9]Ex-JAEA, Japan

E-mail contact of main author: medvedev@a5.kiam.ru

Abstract. Fusion research has to solve the power handling problem toward fusion demonstration reactor (DEMO). A tokamak plasma with negative triangularity and an outboard divertor X-point may offer such an opportunity as an innovative concept. The present paper extends this concept by investigating single null negative triangularity tokamak (SN-NTT). Due to the negative triangularity X-point, internal MHD modes set the pedestal height limit, leading to lower pedestals and possible changes in the ELM regime. On the other hand, the beta limit is relatively low in the NTT. That is connected with the absence of magnetic well for elongated plasma cross-sections. However, negative triangularity tokamak configurations with optimized pressure gradient profiles can be stable for β_N ~3.1 at elongation κ=1.8 and internal inductance l_i=0.9, even in the absence of magnetic well, with the Mercier modes stabilized by magnetic shear with optimal upper triangularity value close to zero in the SN-NTT. Negative triangularity experiments in TCV show a reduction in electron heat transport by a factor two compared with positive triangularity D-shaped configurations, which is partly explained by nonlinear gyrokinetic simulations. Apart from the ELM mitigation and reactor relevant level of beta limits, negative triangularity tokamaks feature other possibilities for power handling such as naturally increased separatrix wetted area due to divertor location at larger radii and more flexible divertor configuration using poloidal field (PF) coils made of NbTi superconductor in the low field region inside the toroidal field (TF) coils. This configuration also allows better pumping accessibility due to larger conductance. Engineering restrictions on the TF coils at the high field side may not allow the TF coil shape conformal to negative triangularity plasma: more realistic race-track shaped TF coils are better compatible with the SN-NTT configuration and superconductor designs using Nb3Sn and Bi-2212 are developed. When ELMs are avoided, stationary heat load on divertor plates can be further reduced by adopting a flux-tube-expansion (FTE) divertor.

1. Introduction

Fusion research has to solve the power handling problem toward fusion demonstration reactor (DEMO). A tokamak plasma with negative triangularity and an outboard divertor X-point may offer such an opportunity as an innovative concept [1-6]. The present paper extends this concept by further investigating single null negative triangularity tokamak (SN-NTT).

The plasma shape beta optimization with positive triangularity tends to lead to the stabilization of high-*n* modes such as ballooning modes, allowing them to enter into the second stability regime. Then, the limiting edge MHD instabilities become medium-*n* peeling-ballooning and low-*n* peeling modes, which result in severe ELM activity damaging the divertor plates. For the case of negative triangularity, the second stability access is closed for the ballooning modes. The destabilization of a whole range of fixed boundary medium- and low-n modes takes place for pedestal heights just above the values for which the Mercier

criterion for localized modes is violated, implying possible changes in the ELM characteristics. Double null negative triangularity tokamak (DN-NTT) configurations feature quite high stable pedestals in the first region of ballooning stability due to high edge shear provided that pedestal current density is low. However, the vertical stability is an issue for the DN-NTT configurations [5]. Already with one outboard X-point in the SN-NTT, internal modes (unstable with fixed boundary condition but localized in the pedestal region) set the pedestal height limit. This limit appears to be much less sensitive to pedestal profile variations and diamagnetic stabilization than the conventional peeling-ballooning mode limits. The changes in ELM regime and Mercier mode driven turbulence are major issues yet to be investigated for the negative triangularity tokamak concept. Studying such phenomena from the first principles would require nonlinear, electromagnetic gyrokinetic simulations. The validation of this theory against experiment, e.g. in the TCV tokamak plasmas with negative triangularity, is still beyond the reach of modern gyrokinetic codes, although recent progress has been made [7]. Plasma pedestal width estimates, in particular, based on the ballooning critical pedestal (BCP) technique used as a proxy for electromagnetic kinetic ballooning mode (KBM) destabilization and corresponding turbulent transport are being explored.

While negative triangularity plasmas have some favorable MHD properties with respect to ELMs, the beta limit is relatively low. That is connected with the absence of magnetic well for elongated plasma cross-sections. On the other hand, well-defined Mercier/ballooning limiting pressure gradient profile exists in the positive shear region and the corresponding beta limit can be readily estimated. The external kink mode stability limit can be obtained by rescaling the ballooning mode limiting profiles. Negative triangularity tokamak configurations with optimized pressure gradient profiles can be stable for $\beta_N \sim 3$ at elongation $\kappa=1.8$ and internal inductance $l_i=0.9$, even in the absence of magnetic well, with Mercier modes stabilized by magnetic shear in the SN-NTT. Of course, the beta limit becomes lower for lower l_i. Fixing the X-point position at the outboard side of the torus and varying the upper triangularity showed that configurations with low values of the upper triangularity are close to the optimal one in terms of external kink mode beta limit.

Engineering restrictions on toroidal field (TF) coils at the high field side may not allow the TF shape conformal to negative triangularity plasma. More realistic race-track shaped TF coils are better compatible with the SN-NTT configuration. The ratio of total poloidal field (PF) coils current to the plasma current necessary to sustain the SN-NTT free boundary equilibrium configuration is close to 5.5, a value close to that of the ITER PF coil system.

Apart from the ELM mitigation and satisfactory level of beta limits, negative triangularity tokamaks feature other possibilities for power handling such as naturally increased separatrix wetted area due to divertor location at larger radii and more flexible divertor configuration using PF coils inside the TF coil made of NbTi superconductor in the low field region [3]. Negative triangularity experiments in TCV show a reduction in electron heat transport by a factor two compared with positive triangularity D-shaped configurations [8], which is partly explained by nonlinear gyrokinetic simulations [7]. This configuration also allows better pumping accessibility due to larger conductance [3]. The flux-tube-expansion (FTE) coils can be also used to further reduce heat load on divertor plates [9].

The free boundary equilibrium and plasma evolution code SPIDER [10] was employed for the PF coil currents fitting given the ballooning optimized profiles of the pressure gradient calculated with the CAXE and BALM codes [11]. The KINX ideal MHD stability code was used to compute the external mode stability with the separatrix at the plasma boundary [12]. The EPED-CH code [13] was used to estimate the pedestal limits in the SN-NTT configuration. Free boundary equilibria with varying currents in the FTE coils were computed

with the EFIT code [14]. The SYSCODE code [15] analysis with the use of updated geometric formulas [16] showed the feasibility of producing a fusion power of 3GW for optimized reactor parameters for the SN-NTT configuration with the plasma current I_p=21MA, torus major/minor radii R_p/a_p=9m/3m, electron density $n_e = 6.5\text{x}10^{19}\text{m}^{-3}$ and the normalized beta β_N=2.1.

2. Free boundary equilibria and divertor solutions

The racetrack shape TF coils were adopted to eliminate the bending stress in the inverted-D shaped coils. The upper plasma triangularity was varied while fixing the lower divertor configuration. The PF coil system layout for the SN-NTT with the following plasma parameters R_p=9m, a_p=3m, I_p=21MA, B_t=5.86T are shown in Fig.1. The inverse free boundary equilibrium problem was solved with the SPIDER code to determine the PF coil currents to maintain the plasma shape close to the target separatrix contour with the separatrix elongation κ=1.8, the upper and lower triangularities δ_u = -0.4, δ_l = -0.9 and fixed position of the X-point with the plasma profiles featuring ballooning mode stability optimized pressure gradient increasing to the boundary [5]. In addition, the plasma boundary is passing through control points at the equatorial plane which determine the aspect ratio. The resulting values of the safety factor and elongation at the 95% of the poloidal flux inside the separatrix are q_{95}=3.0 and κ_{95}=1.73 (Fig. 1a). The ratio of the absolute value sum of the PF coil currents to the plasma current is I_{PF}/I_p = 6.8 in this case. The control point added at the top of the plasma allows one getting the configuration with low upper triangularity deviating from the target contour (Fig. 1b): q_{95}=3.1, κ_{95}=1.71, κ=1.8, δ_u = -0.07. Nevertheless, because of increased weight on the PF currents in the functional minimized when solving the inverse free boundary problem, the ratio I_{PF}/I_p = 5.9 is lower, showing a possibility of overall decrease of PF coil currents to confine the SN-NTT equilibrium with low upper triangularity.

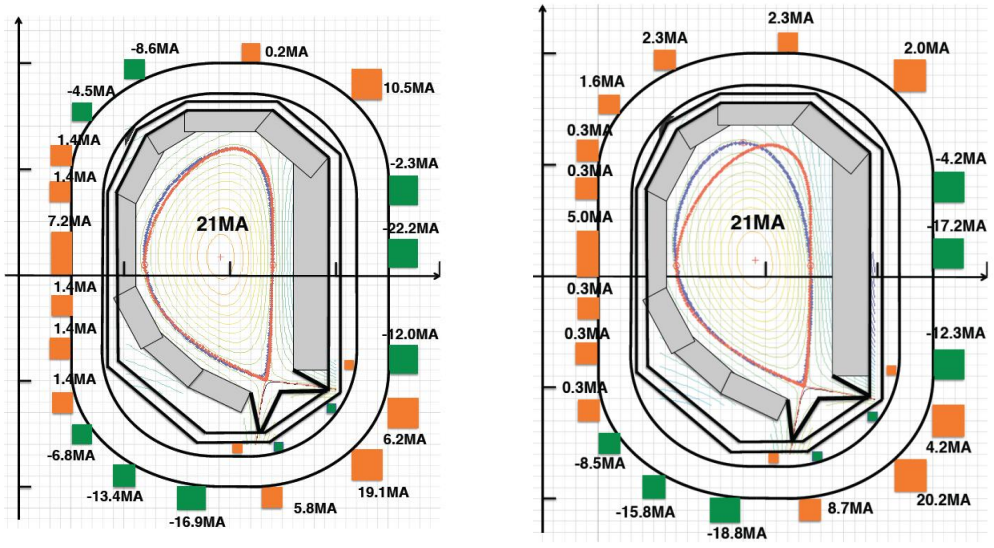

a) *b)*

FIG.1 Free boundary equilibrium configurations with a) δ_u =-0.4, δ_l =-0.9and b) δ_l =-0.07, δ_l =-0.9. The plasma current I_p=21MA. The values of the PF coil currents are given in the plots. The target contour is shown by red dots, the plasma boundary – by blue dots. The circles mark the control points the plasma boundary is passing through. The cross-sections of TF coils and blanket modules are also plotted.

2.1. TF magnet design

The magnet designs of the racetrack shape TF coils are made based on Nb3Sn ITER technology and more advanced Bi-2212 high-Tc superconductor. Basic parameters of TF coils are, coil size of 15m x 20m, number of coils 18, magnetic energy of 170GJ, maximum field of 13.6T, discharge time constant of 15 s, number of turns per coil of 152, coil current of 98kA, number of disks per coil of 7.

Since Nb3Sn is sensitive to strain, use of Nb3Sn in such a big magnet (170GJ) is challenging. Considering Ti has similar thermal expansion coefficient with Nb3Sn, both SS conduit (ITER type) and Ti conduit designs are explored. The use of Ti conduit will reduce total strain of the Nb3Sn conductor [17] and the expected total strain is -0.05%.

Operation of superconducting magnet at higher temperature (~20K) is favorable from the thermal stability of the magnet. In this temperature range, Pb has high thermal capacity and the solder (PbSn) is an appropriate impregnated material [18].

2.2. Free boundary equilibria with FTE divertor

As a "flux-tube-expansion (FTE) divertor" concept [9] has been used to further reduce heat load on divertor plates in DEMO reactors, so the FTE coils can be also applied in SN-NTT for the same purpose. The free boundary equilibria with FTE divertor varying FTE currents (I_{FTE}) were computed using the EFIT code [14]. Fig. 2 shows SN-NTT equilibria with I_p = 21 MA for the same PF coil layout as in Fig. 1 and with the additional FTE coils inside TF coils. Two sets of FTE coils with co-current and counter-current are equipped on the two sides of both divertor legs to expand the flux tube near the inner and outer divertor plates, respectively. The values of currents in other PF coils near the divertor plates are reasonably adjusted to approximately maintain the X-point and separatrix strike point positions during the I_{FTE} turned on.

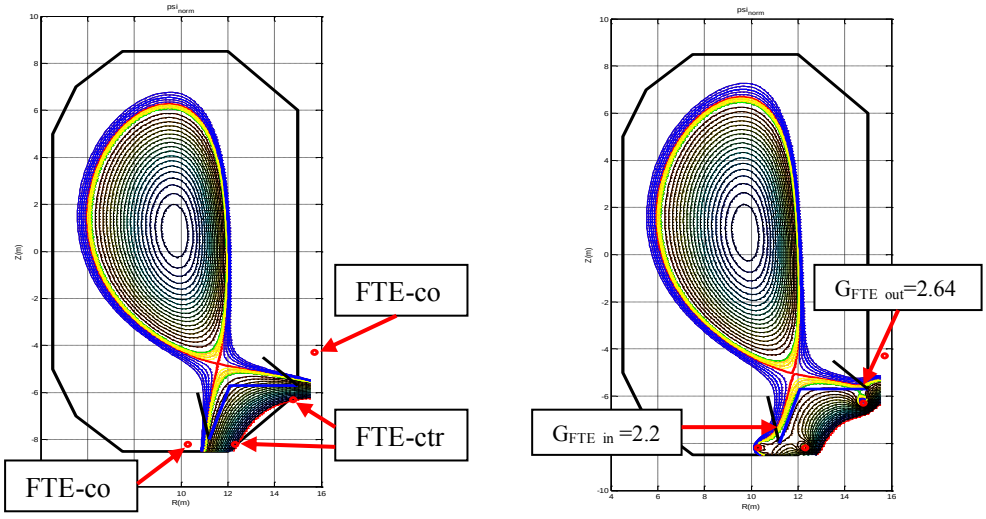

FIG 2. Example of the FTE divertor for a SN-NTT with I_p = 21 MA. Equilibria for (a) I_{FTE} =0MA and (b) I_{FTE} =3MA are shown. The rates of the FTE at the inner and outer strike points are G_{FTE_in} =2.2 and G_{FTE_out} =2.6, respectively.

The rate of the FTE (G_{FTE}) is an important parameter to describe the flux-tube width, which is defined by the inverse of the normalized poloidal field $G_{FTE} = B_{p0}/B_p$ [9], where B_{p0} is the poloidal field at the strike point on the divertor plate for I_{FTE} = 0 and B_p is the poloidal field at the strike point on the divertor plate with non-zero I_{FTE}. Fig. 2b shows an example applying

I_{FTE} = 3 MA. The values of G_{FTE} are about 2.2 and 2.6 for the inner and outer strike points, respectively. Note that this I_{FTE} value is much smaller than the divertor coil current ~ 20 MA (see Fig. 1).

In the original SN-NTT without FTE, the angle α between the magnetic field line and the divertor plate surface is α ≈ 7.2° at outer divertor plate (poloidal tilt angle of 34°) and α ≈ 2.7° at inner divertor plate (poloidal tilt angle of 15°). For the FTE case with I_{FTE} = 3 MA, the angle becomes shallower as α ≈ 2.7° for outer divertor plate and α ≈ 1.3° for inner divertor plate. Further optimization of the FTE coil locations, FTE coil currents, and divertor plate tilting is the future subject. Because the FTE brings not only the expansion of flux tube at the divertor plate but also the extension of connection length and the enlargement of radiation-cooling volume in the divertor region, further reduction of the heat load on the plate is expected over the factor $1/G_{FTE}$. For the quantitative estimation of heat-load reduction, divertor simulation (with the codes like SOLPS, SONIC etc) is also the future subject.

3. Beta limits and vertical stability

Beta limits for the plasma separatrix shapes corresponding to the free boundary equilibria from Fig.1 were investigated. After fixing the plasma boundary an iterative procedure was employed to obtained negative triangularity equilibria with ballooning/Mercier optimized pressure profile [5]. For the NTT equilibria there is no access to the second ballooning stability and a well-defined limiting pressure gradient $p' = dp/d\psi$ exists for fixed profile of parallel current density $J_{||} = < \boldsymbol{J} \cdot \boldsymbol{B} > / < \boldsymbol{B} \cdot \nabla\varphi >$. Several iterations are sufficient to get self-consistent equilibria with ballooning mode limiting p'. For the case corresponding to the shape from Fig.1a, with monotonic q-profile and internal inductance value l_i = 0.84, it gives β_N =3.41 for normalized current $I_N = I_p[MA]/(a[m]B[T])$ = 1.2, I_p =21 MA, B =5.86 T (Fig.3a, dashed shows collisionless bootstrap current density and limiting p' in the corresponding frames). To determine the stability limit against external kink modes, the p' profile is proportionally reduced in a series of fixed boundary equilibria. The stability calculations with the KINX code give n = 1 beta limit of β_N = 2.79 without wall stabilization (lowest value for checked toroidal mode numbers n = 1 – 5, Fig.3b). The mode structure is presented in Fig.3c.

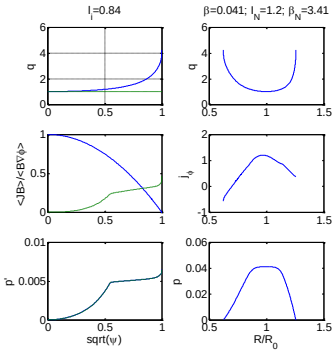

n	β_N
1	2.79
2	3.24
3	3.36
4	3.43
5	3.47
∞	3.41

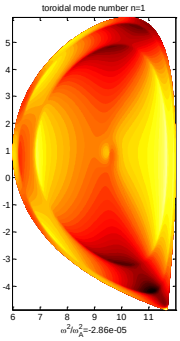

a) *b)* *c)*

FIG.3 a) Plasma profiles in the equilibrium with Mercier/ballooning limiting pressure gradient, l_i=0.84, b) beta limits for different toroidal mode numbers c) the most unstable n=1 mode structure — level lines of the plasma displacement normal to magnetic surfaces.

It turns out that lower upper triangularity SN-NTT plasmas are more stable for the same value of internal inductance: the shear is enhanced due to higher triangularity only very close to the separatrix but can be lower in the plasma bulk. Fig. 4 presents the results of the stability calculations for the case corresponding to the plasma shape in Fig.1b with the ballooning and n=1 limits increased to β_N =3.51 and 3.14 respectively. The beta limits also increase for

higher value of l_i provided that the safety factor at the magnetic axis q_0 is close to 1. For higher l_i=0.93 and normalized current I_N=1 (I_p=17.5MA) the Mercier/ballooning limited value is β_N =3.70 and the n=1 beta limit is β_N =3.3 for the same plasma shape with low upper triangularity. The wall stabilization does not lead to a significant increase in the beta limit because of strong coupling of fixed boundary global Mercier modes to external kink modes: in the latter case with l_i = 0.93 the stabilization with the wall conformal to the plasma boundary, a_w/a = 1.3, gives β_N = 3.63 for n = 1 mode while n > 2 limits are set by internal modes at β_N < 3.7 very close to the localized Mercier mode limit. Decreasing shear (lower l_i) leads to lower beta limits in accordance with the Mercier criterion behavior in the absence of magnetic well.

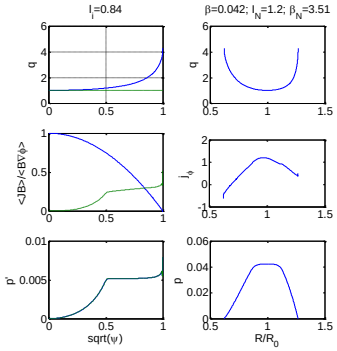

n	β_N
1	3.14
2	3.30
3	3.40
4	3.45
5	3.48
∞	3.51

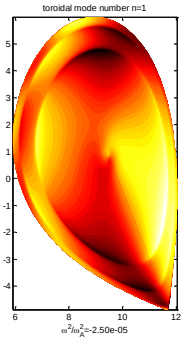

a) *b)* *c)*

FIG.4 a) Plasma profiles in the equilibrium with Mercier/ballooning limiting pressure gradient, l_i=0.84, b) beta limits for different toroidal mode numbers c) the most unstable n=1 mode structure — level lines of the plasma displacement normal to magnetic surfaces.

In contrast to the DN-NTT configurations, for which the double null configuration together with a finite current density at the separatrix provoke strong destabilization of non-rigid modes, the n = 0 vertical stability seems not to be a problem for the SN-NTT. For all the SN-NTT cases considered in this paper the n = 0 growth rates are lower than 15 s^{-1} with the conformal wall at a_w/a = 1.3 with the resistance equivalent to 6cm thick steel as in ITER, which is close to the ITER values.

4. Edge stability and pedestal properties

The edge kink-ballooning mode stability limits usually follow the changes in the high-n limit behavior. Worse localized mode stability leads to lower pressure pedestal height attainable in the negative triangularity configurations and can potentially result in different ELM behavior for positive and negative triangularity configurations. Indeed, changing upper triangularity in TCV plasmas from positive to negative brings an increase in Type I ELM frequency and lower expelled energy per ELM [4].

The pedestal height calculations for the SN-NTT plasma shape close to that in Fig.1a were performed with the recently developed EPED-CH code [13]. For the SN-NTT case with the plasma current I_p=15MA and the pedestal density close to the Greenwald limit $n_{ped} \simeq n_{GW} \simeq 5 \cdot 10^{19} m^{-3}$ (flat density profile with $n_0 / n_{ped} = 1.5, R / L_{n_e} \simeq 1$) the limiting pedestal height is $p_{ped} = 9\, kPa, T_{e,ped} = 0.64\, keV$. This is to be compared to the SN-PTT with the shape mirrored around the plasma center radius R_p (δ>0) for which the corresponding values are about 4 times higher $p_{ped} = 35\, kPa, T_{e,ped} = 2.7\, keV$ at twice as wide pedestal (Fig. 5a). Despite that a good SN-NTT plasma performance with the central temperature T_e = 40 keV and β_N =2.9 is still possible. The corresponding averaged core scale length of the electron temperature gradient R/L_{Te} ~10–12 is compatible with present understanding of core

turbulence. This value can even be lowered if $n_{ped} > n_{GW}$ or with a larger density peaking factor n_0 / n_{ped}. This strong reduction in the pedestal top pressure will likely result in a comparable reduction in the individual ELM energy losses.

The sensitivity of the pedestal height under independent variations of upper and lower triangularity was performed for the SN analytic plasma shapes keeping the SN-NTT reactor relevant geometrical parameters. In Fig.5b the limiting pedestal height is shown versus the average triangularity $\delta = (\delta_u + \delta_l)/2$ under different combinations of upper and lower triangularity. The pedestal pressure p_{ped} seems to depend mostly on the averaged triangularity δ. At constant δ the value of p_{ped} scales unfavorably with the deviation from the symmetric shape $|\delta_u - \delta_l|/2$. These variations are insignificant and the pedestal pressure reaches a minimum if $\delta < -0.2$. The maximum achieved pedestal top pressure is close to 80 kPa which is a factor of 8 larger than the reference SN-NTT case.

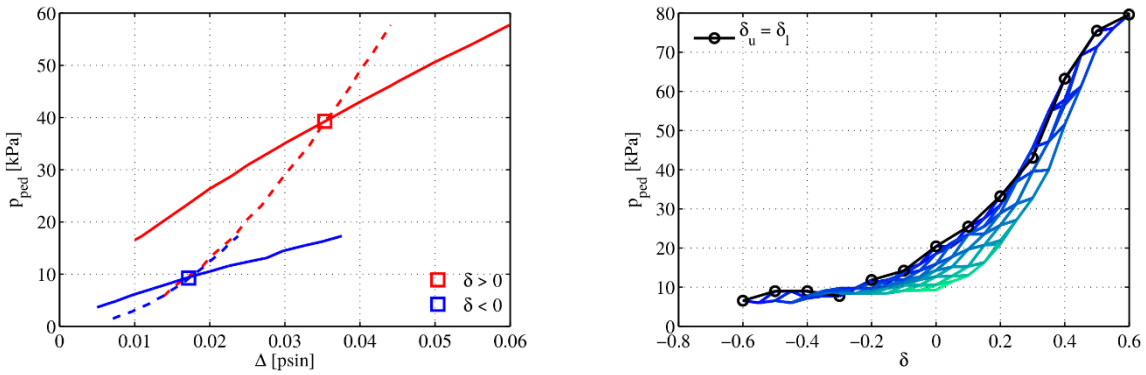

a) *b)*

FIG.5 a) The pedestal pressure limit versus the pedestal width in units of normalized poloidal flux (solid lines) and the pedestal width scaling (dashed), comparison of SN-NTT and SN-PTT cases; b) limiting pressure versus averaged triangularity, the values for the up-down symmetric cases are shown by circles. The color indicates the level of up-down asymmetry with blue corresponding to up-down symmetric cases and green to large differences in the values of the upper and lower triangularity.

5. Discussion

Negative triangularity tokamak configurations with optimized pressure gradient profiles can be stable against external kink modes for reactor relevant values of normalized beta β_N ~3.1. Low upper triangularity SN-NTT configurations seems to be a good candidate for the reactor design being better compatible with the racetrack TF coils and featuring both higher beta limits and better n = 0 stability compared to the DN-NTT.

Internal modes (unstable already with fixed boundary condition but localized in the pedestal region) set the pedestal height limit, which is much less sensitive to diamagnetic stabilization and pedestal profile variations than conventional peeling-ballooning modes. The predicted pedestal height in the NTT is a factor of 4 lower compared to the standard positive triangularity configurations. The averaged core scale length of the electron temperature gradient R/L_{Te} ~10–12 corresponding to β_N ~ 3 is compatible with present understanding of core turbulence. However, further investigations are needed to compute the expected turbulent transport level from first principles. Though the results from linear MHD theory imply changes in the ELM characteristics as compared to positive triangularity configurations, nonlinear studies are really needed. In order to achieve a soft edge beta limit

there is also the need to understand Mercier mode turbulence – a kind of ideal interchange electromagnetic turbulence.

The TCV tokamak with very flexible plasma shape control is very well suited for negative triangularity plasma experiments covering the whole range of principal problems related to the confinement, ELM regimes, scrape-off layer thickness and vertical stability control. Together with supporting experiments from other machines and integrated modeling of reactor relevant scenarios, new experimental campaigns on TCV would provide a substantial ground for the negative triangularity tokamak as innovative confinement concept.

With the theoretical predictions supported by an experiment, a negative triangularity tokamak would become a prospective fusion energy system with other advantages including larger separatrix wetted area, more flexible divertor configuration design, wider trapped particle free SOL, lower background magnetic field for internal poloidal field coils and larger pumping conductance from the divertor room. The experimental evidence of the confinement enhancement in negative triangularity plasmas [8,19] provides a ground for optimism in reaching the reactor relevant normalized beta values $\beta_N > 3$. Bridging the central plasma conditions needed for fusion burning to the associated edge plasma properties would require more theoretical and experimental investigations both of the core and the edge plasma performance as well as reactor studies for negative triangularity tokamaks.

Acknowledgements The work was supported by the grant from the Russian Science Foundation #16-11-10278.

References

[1] M. KIKUCHI, T. TAKIZUKA, Plenary talk at US-EU TTF 2013 (Santa Rosa, USA, 2013), http://ttf2013.ucsd.edu/TTF_Meeting/Presentations.html
[2] M. KIKUCHI, T. TAKIZUKA, M. FURUKAWA, JPS Conf. Proc. **1** (2014) 015014
[3] M. KIKUCHI, et al., 1st International E-Conference on Energies 2014, E002, DOI:10.3390/ECE-1-E002, http://www.sciforum.net/conference/ece-1/paper/2321
[4] A. POCHELON, et al., Plasma Fusion Res. **7** (2012) 2502148
[5] S.YU. MEDVEDEV, M. KIKUCHI et al., Nucl. Fusion **55** (2015) 06301
[6] M. KIKUCHI, S.YU. MEDVEDEV, et al., 42nd EPS Conf. on Plasma Phys. (Lisbon, Portugal, 2015) ECA Vol.39E, P4.179
[7] G. MERLO et al., Plasma Phys. Control. Fusion **57** (2015) 054010
[8] Y. CAMENEN, et al., Nucl. Fusion **47** (2007) 510
[9] T. TAKIZUKA, et al., J. Nucl. Mater. **463** (2015) 1229
[10] A.A. IVANOV, et al., 32nd EPS Conf. on Plasma Phys. (Tarragona, Spain, 2005) ECA Vol.29C, P-5.063
[11] S.YU. MEDVEDEV, et al., 20th EPS Conf. on Contr. Fusion and Plasma Phys. (Lisbon, Portugal, 1993) Vol.17C, part IV, P. 1279
[12] L. DEGTYAREV, et al., Comput. Phys. Commun. **103** (1997) 10
[13] A. MERLE, O. SAUTER, S.YU. MEDVEDEV, "Pedestal properties of H-modes with negative triangularity using the EPED model", submitted to Plasma Phys. Control. Fusion 2016
[14] L.L. LAO, et al., Nucl. Fusion **25** (1985) 1611
[15] D. CHEN, et al., J. Fusion Energ. **34** (2015) 127
[16] O. SAUTER, "Geometric formulas for system codes including the effect of negative triangularity", Fusion Eng. Des., in press 2016 (available online)
[17] T. ANDO, et al., IEEE Trans. Appl. Supercond. **3** (1993) 488
[18] T. ANDO, et al., IEEE Trans. Appl. Supercond. **14** (2004) 1481
[19] O. SAUTER, et al., Phys. Plasmas **21** (2014) 055906